Steel and Composite Structures, *Vol. 23, No. 1 (2017) 1-16*
DOI: https://doi.org/10.12989/scs.2017.23.1.001

Buckling analysis of functionally graded truncated conical shells under external displacement-dependent pressure

Majid Khayat [1a], Davood Poorveis [*1] and Shapour Moradi [2b]

[1] *Department of Civil Engineering, Shahid Chamran University, Ahvaz, Iran*
[2] *Department of Mechanical Engineering, Shahid Chamran University, Ahvaz, Iran*

(Received August 15, 2016, Revised November 13, 2016, Accepted December 03, 2016)

Abstract. This paper is presented to solve the buckling problem of functionally graded truncated conical shells subjected to displacement-dependent pressure which remains normal to the shell middle surface throughout the deformation process by the semi-analytical finite strip method. Material properties are assumed to be temperature dependent, and varied continuously in the thickness direction according to a simple power law distribution in terms of the volume fraction of a ceramic and metal. The governing equations are derived based on first-order shear deformation theory which accounts for through thickness shear flexibility with Sanders-type of kinematic nonlinearity. The element linear and geometric stiffness matrices are obtained using virtual work expression for functionally graded materials. The load stiffness also called pressure stiffness matrix which accounts for variation of load direction is derived for each strip and after assembling, global load stiffness matrix of the shell which may be un-symmetric is formed. The un-symmetric parts which are due to load non-uniformity and unconstrained boundaries have been separated. A detailed parametric study is carried out to quantify the effects of power-law index of functional graded material and shell geometry variations on the difference between follower and non-follower lateral buckling pressures. The results indicate that considering pressure stiffness which arises from follower action of pressure causes considerable reduction in estimating buckling pressure.

Keywords: buckling; displacement dependent pressure; semi-analytical finite strip; FGM shells

1. Introduction

Structures are subjected to wide variety of forces, which can be classified into two categories: (a) conservative forces; and (b) non-conservative forces. Stability of structures under deformation-dependent loads (follower forces) depending on the loading type, body attached or space attached, load distribution and shell boundary conditions can be categorized under conservative or non-conservative title. In the case of conservative loads static criterion (divergence) can be used which finally produces symmetric global stiffness matrix. Non-conservativeness of loads can cause the system be divided into purely or hybrid non-conservative. The first group only fails by flutter and so the kinetic criterion which connects computing buckling loads to vibration equation of structure, governs. In the hybrid case both criteria, static or kinetic, can dominate the problem (Datta and Biswas, 2011 Argyris and Symeonidis, 1981).

Functionally Graded Material (FGM) belongs to a class of advanced material characterized by variation in properties as the dimension varies. Currently, FGMs have been widely applied in aerospace and nuclear industries. The overall properties of FMG are unique and different from any of the individual material that forms it. There is a wide range of applications for FGM and it is expected to increase as the cost of material processing and fabrication processes are reduced by improving these processes. Pure metals are of little use in engineering applications because of the demand of conflicting property requirement (Rasheedat and Akinlabi 2012).

Bolotin (1963) was one of the pioneering researches who extensively investigated the effects of load behavior on stability of structures. He divided the loads into dead and follower types. In another study on conservativeness of a normal pressure field acting on a shell, Cohen (1966) while confirming the Bolotin's result for flat plates generalized the result to a non-uniform continuous normal pressure field acting on an arbitrary shell. Hibbitt (1979) derived the contribution of follower forces to the tangent stiffness matrix and called it load stiffness matrix. He showed that this matrix is in general un-symmetric but in special cases leads to symmetric one. Longanathan *et al.* (1979) investigated the effects of follower forces in the finite element analysis of stability problems. Schweizerhof and Ramm (1984) discussed on displacement dependent pressure loads in nonlinear finite element analysis. They discussed in detail the conditions when a pressure load is conservative and when it is not. The important part of their work was the classification of loads into body attached and

*Corresponding author, Ph.D., Professor,
E-mail: dpoorveis@scu.ac.ir
[a] Ms.C. Student, E-mail; khayatmajid@yahoo.com
[b] Ph.D., Professor, E-mail: moradis@scu.ac.ir

http://www.techno-press.org/?journal=scs&subpage=6 ISSN: 1229-9367 (Print), 1598-6233 (Online)

space attached loads. Poorveis and Kabir (2006) estimated buckling of discretely stringer-stiffened composite cylindrical shells under combined axial compression and external pressure in the form of live (follower) pressure. Cagdas and Adali (2011) investigated buckling of cross-ply cylinders under hydrostatic pressure by considering pressure stiffness by semi analytical finite element method. They estimated the effects of taking pressure stiffness into account for different shell lay-ups and geometries. Khayat *et al*. (2016) investigated the effect of pressure stiffness on buckling of thick deep shells.

Many investigations have been carried out on the buckling analysis of FG rectangular plates shells from which some nearly published are reviewed here. Torki *et al*. (2014) investigated behavior of functionally graded cylindrical shells under an end axial follower force. The material properties were assumed to be graded along the thickness direction according to a simple power law. Shen (2002) studied a post buckling analysis for a functionally graded cylindrical panel of finite length subjected to axial compression in thermal environment. Material properties were assumed to be temperature dependent, and graded in the thickness direction according to a simple power law distribution in terms of the volume fractions of the constituents. Na and Kim (2004) analyzed three-dimensional thermal buckling of functionally graded materials. Lanhe (2004) presented a closed-form solution for the thermal buckling of a simply supported moderately thick rectangular plate made of functionally graded materials. Chi and Chung (2006) examined the mechanical behavior of FGM plates under transverse properties were assumed to be temperature dependent, and varied continuously in the thickness direction according to a simple power law distribution in terms of the volume fraction of a ceramic and metal. Reddy and Chin (2007) analyzed the dynamic thermo elastic response of functionally graded cylinders and plates. Thermo mechanical coupling was included in the formulation, and a finite element model of the formulation was developed. Ganapathi (2007) studied the dynamic stability behavior of clamped FGM spherical shell structures subjected to external pressure. The material properties were graded in the thickness direction according to the power-law distribution in terms of volume fractions of the constituents of the material. Santos *et al*. (2008) used semi-analytical axisymmetric finite element model for thermo-elastic analysis of functionally graded cylindrical shells subjected to transient thermal shock loading. The three-dimensional equations of motion were reduced to two-dimensional ones by expanding the displacement field in Fourier series in the circumferential direction involving circumferential harmonics. Sofiyev (2010) investigated the elastic buckling of FGM truncated thin conical shells under combined axial tension and hydrostatic pressure. Tornabene *et al*. (2014) investigated free vibration of free-form doubly-curved shells made of functionally graded materials. They used higher-order equivalent single layer theories. Dung and Hoa (2015) investigated the nonlinear buckling and post-buckling of functionally graded stiffened thin circular cylindrical shells surrounded by elastic foundations in thermal environment and under torsional load by analytical approach. Bich *et al*. (2016) presented an analytical approach to investigate non-linear buckling analysis and post-buckling behavior of FGM toroidal shell segments filled inside by an elastic medium under external pressure loads including temperature effects. Chaht *et al*. (2015) investigated the bending and buckling behaviors of size-dependent nanobeams made of functionally graded materials (FGMs) including the thickness stretching effect. The size-dependent FGM nanobeam was investigated on the basis of the nonlocal continuum model. Duc *et al*. (2015) presented an analytical approach on the nonlinear response of thick functionally graded circular cylindrical shells with temperature independent material property surrounded on elastic foundations subjected to mechanical and thermal loads. Material properties were graded in the thickness direction according to a sigmoid power law distribution in terms of the volume fractions of constituents (S-FGM). Zhang *et al*. (2015) studied buckling of elasto-plastic FGM cylindrical shells under combined axial compression and external pressure with classical shell theory. Viola *et al*. (2016) investigated the static behavior of functionally graded spherical shells and panels subjected to uniform loadings at the extreme surfaces. The free vibration analysis was performed by Fantuzzi *et al*. (2016) for spherical and cylindrical shells with one-layered FGM structures and sandwich structures embedding an internal FGM core.

In a word, most of the previous studies on the buckling of FGM shells have been performed under non-follower pressure. Nearly most of researches related to considering pressure stiffness effects on stability problems were restricted to laminated composite cylindrical shells or panels and no investigations have been carried out on the buckling behavior of functionally graded shells under external follower pressure. So, the authors of this paper intend to study the behavior of functionally graded conical shells subjected to follower load by semi-analytical finite strip method. The important points of the present study are summarized as follows:

- To demonstrate the accuracy and validity of the proposed method, the buckling load for the shell has been compared with other published researches.
- The exact expression for calculating the stiffness matrix due to the follower pressure for general shell of revolution is derived.
- The effects of considering pressure stiffness matrix on the magnitude of the buckling pressure for various shells are investigated.
- The effects of various parameters such as power-law index of functionally graded material, length and thickness of shell and shell boundary conditions interacting with loading type on shell buckling pressure are examined.
- The regions of divergence and flutter criteria applicability for truncated conical shell are detected.
- Despite existing un-symmetric global stiffness matrix in some cases, all analyses are based on static (divergence) criterion.

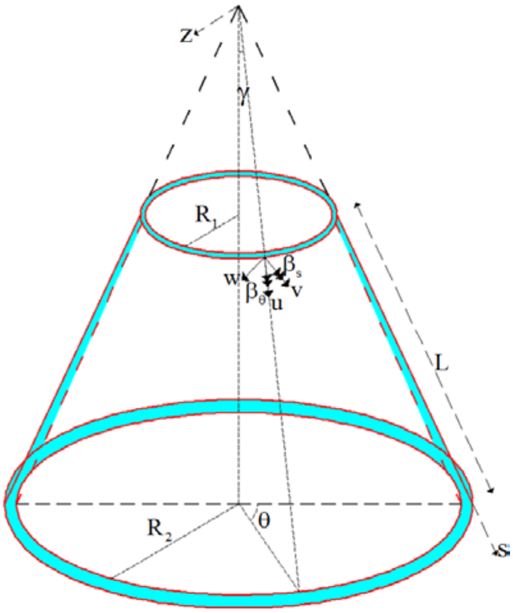

Fig. 1 Geometry of the FG truncated conical shell

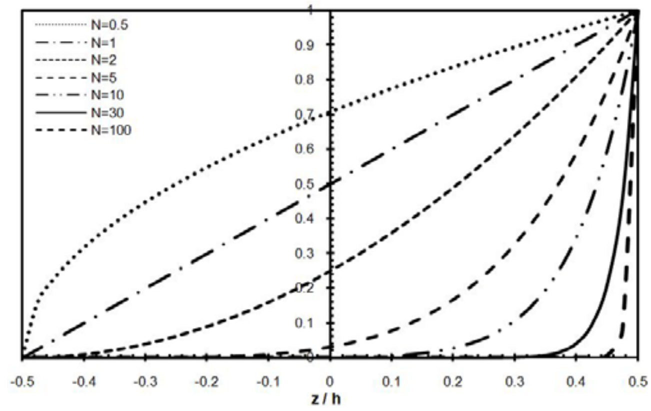

Fig. 2 Variation of volume fraction through shell thickness for various values of the power-law index N

2. Theoretical development

2.1 Formulation of the problem

The geometry of the system is defined in Fig. 1. We consider a FG truncated conical shell with generator length L, radii R_1 of the smaller end and R_2 of the larger end, the total thickness h and semi-vertex angle γ of the generator to the height of cone. The coordinate system (s, θ, z) is also shown in Fig. 1, where the s-axis in the direction of the generator of the cone, the z-axis in the direction normal to the reference surface of the cone, and θ-axis in the normal direction to the s-z plane, form an orthogonal curvilinear coordinates system. The displacement components of the middle surface are u, v and w along the meridian, tangential and lateral directions and β_s, β_θ are the rotations around the θ and s axes, respectively.

It is assumed that the FGM conical shell is made of a mixture of a metal phase (denoted by m) and a ceramic phase (denoted by c), with the material composition varying smoothly along its thickness direction only. Thus, the material properties of FGMs, like Young's modulus E or Poisson's ratio v, can be expressed as (Sofiyev 2010)

$$F_{eff}(z) = F_m V_m(z) + F_c V_c(z) \tag{1}$$

where F_{eff} is the effective mechanical or physical property and F_m and F_c are the material properties of the ceramic and metal, respectively, and may be expressed as a function of temperature

$$F_{eff}(T) = F_0(F_{-1}T^{-1} + 1 + F_1T + F_2T^2 + +F_3T^3) \tag{2}$$

in which T = 300 K (room temperature), F_0, F_{-1}, F_1, F_2 and F_3 are the coefficients of temperature T(K) expressed in Kelvin and are unique to the constituent materials (Sofiyev 2010). Also, V_m and V_c stand for the volume fractions of metal and ceramic, respectively that are related by

$$V_m(z) + V_c(z) = 1 \tag{3}$$

The ceramic phase has greater elasticity modulus and lower density and Poisso's ratio compared to the metal phase (Viola *et al*. 2016). V_m can be expressed by the power law

$$V_m = \left(\frac{z}{h} + \frac{1}{2}\right)^N, N \geq 0 \tag{4}$$

where N is the power law exponent, which is a critical parameter to control the distribution of the constituents. The variations of the volume fraction of metal in the thickness direction for a FGM shell with different volume fraction functions have been drawn in Fig. 2. The vertical-axis stands for the volume fraction while horizontal-axis represents the position along the thickness of an FGM conical shell. In this study, the temperature has been assumed to be equal to the reference temperature (the environment temperature), i.e., 300 K.

The vector of stress resultants is defined as

$$\sigma^T = \{N_{ss}\ \ N_{\theta\theta}\ \ N_{s\theta}\ \ M_{ss}\ \ M_{\theta\theta}\ \ M_{s\theta}\ \ Q_{sz}\ \ Q_{\theta z}\}^T \tag{5}$$

N_{ss}, $N_{\theta\theta}$, $N_{s\theta}$ are the in-plane meridional, circumferential and shearing force resultants per unit length, respectively. M_{ss}, $M_{\theta\theta}$, $M_{s\theta}$ are the analogous couples, while Q_{sz}, $Q_{\theta z}$ are the transverse shear force resultants per unit length. The constitutive equation relates internal stress resultants and couples to generalized strain components on the middle surface

$$\begin{Bmatrix} N_{ss} \\ N_{\theta\theta} \\ N_{s\theta} \\ M_{ss} \\ M_{\theta\theta} \\ M_{s\theta} \\ Q_{sz} \\ Q_{\theta z} \end{Bmatrix} = \int_{-h/2}^{h/2} \begin{Bmatrix} \sigma_{ss} \\ \sigma_{\theta\theta} \\ \tau_{\theta s} \\ z\sigma_{ss} \\ z\sigma_{\theta\theta} \\ z\tau_{\theta s} \\ \tau_{sz} \\ \tau_{\theta z} \end{Bmatrix} dz = \begin{bmatrix} [A] & [B] & 0 \\ [B] & [D] & 0 \\ 0 & 0 & [H] \end{bmatrix} \begin{Bmatrix} \varepsilon_{ss} \\ \varepsilon_{\theta\theta} \\ \gamma_{s\theta} \\ k_{ss} \\ k_{\theta\theta} \\ k_{s\theta} \\ \gamma_{sz} \\ \gamma_{\theta z} \end{Bmatrix} \tag{6}$$

A_{ij} is extensional stiffness, D_{ij} is bending stiffness and B_{ij} is bending-extensional coupling stiffness and are defined as (Torki *et al*. 2014)

$$\begin{aligned}
&\left(A_{ij},B_{ij},D_{ij}\right)=\int_h\left(1,z,z^2\right)S_{ij}(z)dz \quad i\,,j=1,2,6\\
&H_{ij}=K_s\int_h S_{ij}(z)dz \quad i\,,j=4,5\\
&S_{11}=S_{22}=\frac{E(z)}{1-\upsilon(z)^2} \qquad S_{12}=S_{21}=\frac{\upsilon(z)E(z)}{1-\upsilon(z)^2}\\
&S_{44}=S_{55}=S_{66}=\frac{E(z)}{2(1+\upsilon(z))}
\end{aligned} \tag{7}$$

where K_s is the shear correction factor. $E(z)$ and $v(z)$ must be determined using Eqs. (1) and (4).

2.2 Semi analytical Finite strip method

To approximate displacements and rotations in the shell middle surface, two types of interpolation functions are used in this method. In the circumferential direction which geometry and material properties of the shell are constant, Fourier series are taken into account, while in meridional direction Lagrangian functions which may have two or more nodes have been used. The circumferential variation of the global displacements u, v, w, β_s and β_θ can be described by a suitable Fourier series expansion which in general consists of both sine and cosine terms

$$\Delta(s,\theta)=\Delta^o(s)+\sum_{k=1}^{NH}\left[\Delta^{c_n}(s)\cos(kn\theta)+\Delta^{s_n}(s)\sin(kn\theta)\right] \tag{8}$$

with

$$\Delta=[u\ v\ w\ \beta_s\ \beta_\theta]^T \tag{9}$$

where k represent an integer number varying from 1 to number of harmonics, NH. Also n is circumferential wave number which minimize buckling load. Discretization of $\Delta(s)$ in the meridional direction is carried out by using Lagrangian interpolation functions of different orders

$$\Delta(s)=\sum_{i=1}^{NN}\Delta_i N_i(s) \tag{10}$$

In which, $N_i(s)$ stands for Lagrangian shape function and Δ_i contains displacement and rotation components of ith node. Also, NN, represents number of nodes in each strip in the meridional direction. Combining Eqs. (8) and (10) gives

$$\begin{aligned}
&\Delta(s,\theta)=\sum_{i=1}^{NN}\Delta_i^o N_i(s)\\
&+\sum_{k=1}^{NH}\sum_{i=1}^{NN}[\Delta_i^{cn}N_i(s)\cos(kn\theta)+\Delta_i^{sn}N_i(s)\sin(kn\theta)]
\end{aligned} \tag{11}$$

in Eq. (11), Δ_i^o, Δ_i^{cn} and Δ_i^{sn} are unknown coefficients vectors related to nodal i of each closed strip.

2.3 Strain-displacement relationships

The strain in an arbitrary point and with distance z from mid-surface can be expressed in terms of mid-surface strains ε_{ss}, $\varepsilon_{\theta\theta}$ and $\gamma_{s\theta}$ and also mid-surface changes of curvatures k_{ss}, $k_{\theta\theta}$ and $k_{s\theta}$

$$\bar{\varepsilon}_{ss}=\varepsilon_{ss}+zk_{ss} \qquad \bar{\varepsilon}_{\theta\theta}=\varepsilon_{\theta\theta}+zk_{\theta\theta} \qquad \bar{\gamma}_{s\theta}=\gamma_{s\theta}+zk_{s\theta} \tag{12}$$

The generalized strain vector which plays an important role in the stress-strain relationships is

$$\varepsilon=\{\varepsilon_{ss}\ \varepsilon_{\theta\theta}\ \gamma_{s\theta}\ k_{ss}\ k_{\theta\theta}\ k_{s\theta}\ \gamma_{\theta z}\ \gamma_{sz}\} \tag{13}$$

in which linear strains of mid-surface, ε_{ss}, $\varepsilon_{\theta\theta}$ and $\gamma_{s\theta}$ are defined in terms of displacements as

$$\begin{aligned}
&\varepsilon_{ss}=\frac{\partial u}{\partial s}\\
&\varepsilon_{\theta\theta}=\frac{1}{R}\left(\frac{\partial v}{\partial\theta}+u\cos\varphi+w\sin\varphi\right)\\
&\gamma_{s\theta}=\frac{\partial v}{\partial s}+\frac{1}{R}\frac{\partial u}{\partial\theta}-\frac{v\cos\varphi}{R}
\end{aligned} \tag{14}$$

The non-linear part of mid-surface strains based on Sanders's (1963) non-linear shell theory is as follows

$$\begin{aligned}
&\varepsilon_{ss}^{NL}=\frac{1}{2}\left(\frac{\partial w}{\partial s}\right)^2+\frac{1}{2}\left(\frac{1}{2R}\left(R\frac{\partial v}{\partial s}+v\cos\varphi-\frac{\partial u}{\partial\theta}\right)\right)^2\\
&\varepsilon_{\theta\theta}^{NL}=\left(\frac{1}{2R}\left(\frac{\partial w}{\partial\theta}-v\sin\varphi\right)\right)^2\\
&\qquad+\frac{1}{2}\left(\frac{1}{2R}\left(R\frac{\partial v}{\partial s}+v\cos\varphi-\frac{\partial u}{\partial\theta}\right)\right)^2\\
&\gamma_{s\theta}^{NL}=\frac{1}{R}\left(\frac{\partial w}{\partial s}\right)\left(\frac{\partial w}{\partial\theta}-v\sin\varphi\right)
\end{aligned} \tag{15}$$

Bending curvatures strains, k_{ss} and $k_{\theta\theta}$ and torsional curvature, $k_{s\theta}$ are

$$\begin{aligned}
&k_{ss}=\frac{\partial\beta_s}{\partial s}\\
&k_{\theta\theta}=\frac{1}{R}\left(\frac{\partial\beta_\theta}{\partial\theta}+\beta_s\cos\varphi\right)\\
&k_{s\theta}=\frac{\partial\beta_\theta}{\partial s}-\frac{\beta_s}{R}\cos\varphi+\frac{1}{R}\frac{\partial\beta_s}{\partial\theta}+\frac{1}{2}\left(\frac{v}{R}\cos\varphi+\frac{\partial v}{\partial s}\right)\left(\frac{\sin\varphi}{R}\right)
\end{aligned} \tag{16}$$

and based on first order shear deformation theory, transverse shear strains are

$$\begin{aligned}
&\gamma_{sz}=\beta_s+\frac{\partial w}{\partial s}\\
&\gamma_{\theta z}=\beta_\theta+\frac{1}{R}\frac{\partial w}{\partial\theta}-\frac{v}{R}\sin\varphi
\end{aligned} \tag{17}$$

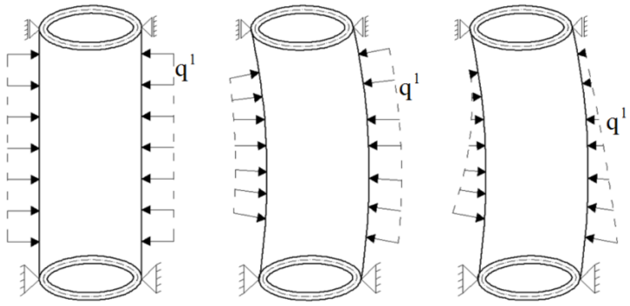

Fig. 3 Loads definition

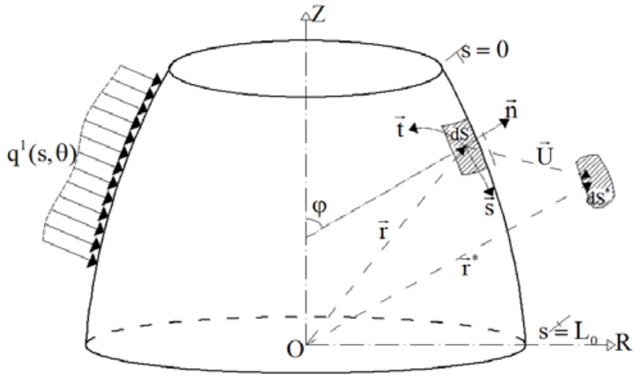

Fig. 4 Deformation of an elemental area

2.4 Linear elastic and geometric stiffness matrices

The linear part of internal virtual work of shell is as follows

$$\delta W_{int}^{L} = \iiint_{s\,\theta\,t} \left(\sigma_{ss}\delta\varepsilon_{ss} + \sigma_{\theta\theta}\delta\varepsilon_{\theta\theta} + \tau_{s\theta}\delta\gamma_{s\theta} + \tau_{sz}\delta\gamma_{sz} + \tau_{\theta z}\delta\gamma_{\theta z}\right) R dz d\theta ds \tag{18}$$

integration of Eq. (18) in the thickness direction and by using Eq. (6), the internal virtual work can be written

$$\delta W_{int}^{L} = \int_0^{l_o}\int_0^{2\pi} (N_{ss}\delta\varepsilon_{ss} + N_{\theta\theta}\delta\varepsilon_{\theta\theta} + N_{s\theta}\delta\gamma_{s\theta} + M_{ss}\delta k_{ss} + M_{\theta\theta}\delta k_{\theta\theta} + M_{s\theta}\delta k_{s\theta} + Q_{sz}\delta\gamma_{sz} + Q_{\theta z}\delta\gamma_{\theta z}) R d\theta ds \tag{19}$$

in which l_o is the length of shell generator. Discretization of $\delta W_{\text{int}}^{L}$ by using Eq., (19) gives

$$\delta W_{int}^{L} = \sum_{j=1}^{nstrip} (\delta\Delta_j)^T K_{ej} \Delta_j \tag{20}$$

in this equation, $\hat{\Delta}_j$ contains all unknown coefficients of displacements and rotations of jth strip and $\delta\hat{\Delta}_j$ represents its virtual counterpart, also K_{ej} is the linear stiffness matrix of jth strip.

To form geometric or initial stress stiffness matrix, it is required to carry out a pre-buckling static analysis to obtain in-plane forces, N^o_{ss}, $N^o_{\theta\theta}$ and $N^o_{s\theta}$ for each strip in the gauss points. Then the internal works of these real membrane forces in non-linear virtual strains are in the form

$$\delta W_{int}^{NL} = \iint_{s\,\theta} \left(N^o_{ss}\delta\varepsilon^{NL}_{ss} + N^o_{\theta\theta}\delta\varepsilon^{NL}_{\theta\theta} + N^o_{s\theta}\delta\gamma^{NL}_{s\theta}\right) R d\theta ds \tag{21}$$

discretization of $\delta W_{\text{int}}^{L}$ by using Eq., (21) gives

$$\delta W_{int}^{NL} = \sum_{j=1}^{nstrip} (\delta\Delta_j)^T K_{Gj} \Delta_j \tag{22}$$

in which K_{Gj} represents the geometric stiffness matrix of jth strip. Assembling of K_{ej} and K_{Gj} of all strips result in global linear elastic stiffness matrix, K_e and global geometric stiffness matrix, K_G for the shell.

2.5 Load-dependent stiffness

Schweizerhof and Ramm (1984) divided Loads in two groups, body attached and space attached. In the space attached category both direction and magnitude of the loads change during acting on structure but in the body attached group only direction of loading action changes (Fig. 3), the following assumption are have been made:

- The direction of applied loads before and after deformation is perpendicular to the shell
- Loading acts on the middle surface
- Strains of the shell are small
- Pressures are body attached

In Fig. 4, position vector of an arbitrary point in the middle surface of conical shell denoted by $\vec{r}$, and $\vec{U}$ represents displacement vector of the point. So, the position vector in the deformed state is

$$\vec{r}^* = \vec{r} + \vec{U} \tag{23}$$

The components of $\vec{r}$ and $\vec{U}$ in terms of orthogonal curvilinear system (s, θ, z) are as follows

$$\begin{aligned} \vec{r} &= (R\sin\gamma - Z\cos\gamma)\vec{s} + (R\cos\gamma - Z\sin\gamma)\vec{n} \\ \vec{U} &= u(s,\theta)\vec{s} + v(s,\theta)\vec{t} + w(s,\theta)\vec{n} \end{aligned} \tag{24}$$

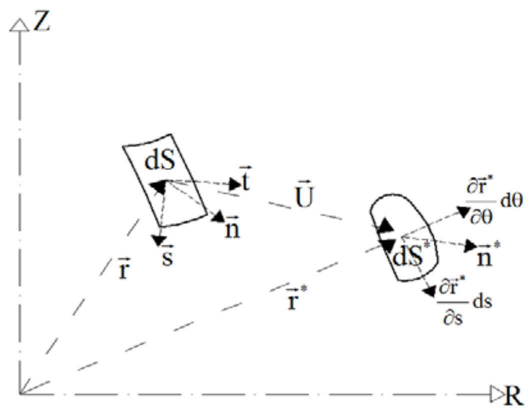

Fig. 5 Tangential and normal vectors to the un-deformed and deformed surfaces

In which R and Z are defined in Fig. 4, and γ is semi apex angle of cone, $\vec{n}$ represents unit normal vector to the shell un-deformed middle surface, $\vec{t}$ is unit vector in the circumferential direction and $\vec{s}$ shows unit vector in the meridianal direction, both in un-deformed states.

The external virtual work of distributed follower external pressure, $q^1(s, \theta)$, is

$$\delta W_{ext}^{ql} = -\iint_S (q^1(s,\theta) dS^* \vec{n}^*).\delta\vec{U} \tag{25}$$

In which, $q^1(s, \theta)$ can be non-uniform in both directions, s and θ, but it is assumed to be continuous function of s and θ. dS^* is elemental area in the deformed state and $\vec{n}^*$ defines unit normal vector to the deformed shell middle surface. Also, $\delta\vec{U}$ reflects infinitesimal virtual displacement vector of shell middle surface. According to vector analysis the product of normal vector and differential element of deformed mid-surface area can be written as

$$dS^*\vec{n}^* = \frac{\partial\vec{r}^*}{\partial s} ds \times \frac{\partial\vec{r}^*}{\partial\theta} d\theta \tag{26}$$

in which, the notation 'x' stands for vector product. Expansion of Eq. (26) gives

$$dS^*\vec{n}^* = \begin{vmatrix} \vec{s} & \vec{t} & \vec{n} \\ \frac{\partial r_s^*}{\partial s} & \frac{\partial r_\theta^*}{\partial s} & \frac{\partial r_z^*}{\partial s} \\ \frac{\partial r_s^*}{\partial\theta} & \frac{\partial r_\theta^*}{\partial\theta} & \frac{\partial r_z^*}{\partial\theta} \end{vmatrix} ds d\theta \tag{27}$$

To concise the relation 27, the following derivatives can be utilized

$$\begin{aligned} &\frac{\partial Z}{\partial s} = -\cos\gamma \qquad \frac{\partial R}{\partial s} = \sin\gamma \\ &\frac{\partial\vec{n}}{\partial s} = \frac{1}{R_1}\vec{s} \qquad \frac{\partial\vec{s}}{\partial s} = -\frac{1}{R_1}\vec{n} \\ &\frac{\partial\vec{t}}{\partial\theta} = -\vec{n}\cos\gamma - \vec{s}\sin\gamma \qquad \frac{\partial\vec{s}}{\partial\theta} = \sin\gamma\vec{t} \\ &\frac{\partial\vec{n}}{\partial\theta} = \cos\gamma\vec{t} \qquad \frac{\partial}{\partial s} = \frac{1}{R_1}\frac{\partial}{\partial\varphi} \end{aligned} \tag{28}$$

in which γ is semi apex angle of cone as illustrated in Fig. 1. Finally by using the above relations, the virtual work generated by distributed follower external pressure is

$$\delta W_{ext}^{ql} = -\int_0^{2\pi}\int_0^{l_0} q^1(s,\theta) \begin{vmatrix} \delta u & \delta v & \delta w \\ 1+\frac{\partial u}{\partial s} & \frac{\partial v}{\partial s} & \frac{\partial w}{\partial s} \\ \frac{1}{R}(\frac{\partial u}{\partial\theta} - v\sin\gamma) & 1+\frac{1}{R}\frac{\partial v}{\partial\theta}+\frac{u}{R}\sin\gamma+\frac{w}{R}\cos\gamma & \frac{1}{R}(\frac{\partial w}{\partial\theta} - v\cos\gamma) \end{vmatrix} dS \tag{29}$$

The external virtual work of displacement-dependent non-uniform pressure includes expressions of first, second and third order of displacements and their derivatives. The first order terms directly form external load vector which can be used in the pre-buckling analysis and the higher order terms incorporate in the geometrical nonlinear analysis. To form pressure stiffness matrix due to arbitrary non-uniform continuous follower pressure, $q(s, t)$, which is suitable for linearized buckling analysis only quadratic terms of deformations should be kept. Then integrate by parts Eq. (29) to reach the following subdivided symmetric and skew-symmetric expressions

$$\begin{aligned} \delta W_{sym}^{domain} = -\delta\iint_S \frac{1}{2} q^1(s,\theta)(&\frac{v^2}{R}\cos\gamma + \frac{w^2}{R}\cos\gamma \\ &+\frac{w}{R}\frac{\partial v}{\partial\theta} - \frac{v}{R}\frac{\partial w}{\partial\theta} + \frac{w}{R}\frac{\partial}{\partial s}(R.u) - u\frac{\partial w}{\partial s}) R ds d\theta \end{aligned} \tag{30}$$

$$\begin{aligned} \delta W_{skew-sym}^{load} = &-\frac{1}{2}\iint_S w\delta v \frac{\partial q^1(s,\theta)}{\partial\theta} ds d\theta \\ &+\frac{1}{2}\iint_S v\delta w \frac{\partial q^1(s,\theta)}{\partial\theta} ds d\theta - \frac{1}{2}\iint_S w\delta u \frac{\partial q^1(s,\theta)}{\partial s} ds d\theta \\ &+\frac{1}{2}\iint_S u\delta w \frac{\partial q^1(s,\theta)}{\partial s} ds d\theta \end{aligned} \tag{31}$$

$$\begin{aligned} \delta W_{skew-sym}^{boundary} = &-\frac{1}{2}\int_0^{2\pi}\left[Ru\delta w q^1(s,\theta)\right]_0^{l_0} d\theta \\ &+\frac{1}{2}\int_0^{2\pi}\left[Rw\delta u q^1(s,\theta)\right]_0^{l_0} d\theta + \frac{1}{2}\int_0^{l_0}\left[w\delta v q^1(s,\theta)\right]_0^{2\pi} ds \\ &-\frac{1}{2}\int_0^{l_0}\left[v\delta w q^1(s,\theta)\right]_0^{2\pi} ds \end{aligned} \tag{32}$$

in which Eq. (30) represents symmetric part of external virtual work. Also, the other two parts, Eqs. (31) and (32) are related to load non-uniformity and boundaries of the shell, respectively. They are anti-symmetric bi-linear forms and upon discretization lead to skew-symmetric matrices which bring about un-symmetry of total load stiffness matrix. In the present study both types of un-symmetry are present and loading can be non-uniform in meridional and circumferential directions. It should be noted that for conical shell due to closed shape in circumferential direction and continuity of loading, the two last terms in the Eq. (32) are omitted.

Discretization of Eq. (32) for each closed strip causing the related stiffness matrix be un-symmetric due to boundaries of the strip, but continuity of displacements and loading in the common lines of adjacent strips leads to omitting this un-symmetry upon assembling process and forming global matrix. It is to be noted that only in the boundary nodal lines the aforementioned un-symmetry remains and as noted in previous researches, in special boundary conditions this un-symmetry is also disappeared.

Fig. 6 describes the physical meaning of different boundary and load conditions and their effects on the categorization of the related system. The system in Fig. 6(a)

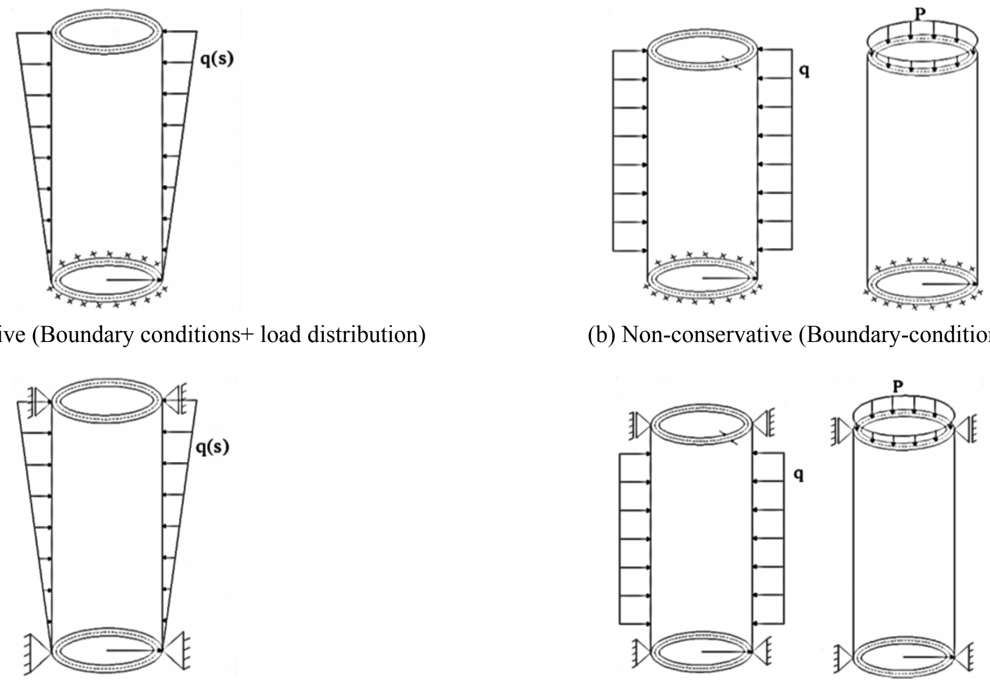

(a) Non-conservative (Boundary conditions+ load distribution) (b) Non-conservative (Boundary-condition)

(c) Non-conservative (Load distribution) (d) Conservative

Fig. 6 Boundary and load conditions

is non-conservative because load is non-uniform and end of shell can move along horizontal direction. In the second structure, Fig. 6(b), despite uniformity of applied loading, lateral or axial, the free end causes the system to be non-conservative. Despite the structure in Fig. 6(c), has support conditions leading to vanishing boundary terms according to Eq. (32) but It is non-conservative still because load distribution is non-uniform. Fig. 6(d) represents conservative systems, loading is uniform and the boundaries have been sufficiently restrained.

If the pressure stiffness matrix is symmetric, the corresponding is called conservative. Otherwise, if pressure is un-symmetric, the system is termed as non-conservative. In the case of conservative which finally leads to symmetric global stiffness matrix, static criterion (divergence) can be used. Non-conservativeness of loads can cause the system be divided into purely or hybrid non-conservative. The first group only fails by flutter and so the kinetic criterion which connects computing buckling loads to vibration equation of structure, governs. In the hybrid case both criteria, static or kinetic, can dominate the problem. In commercial programs such as Abaqus pressure stiffness matrix stored symmetric (Goyal and Kapania 2008, Abaqus/standard user's manual 1998).

2.6 Linearized buckling analysis

Having been formed global linear elastic stiffness matrix, K_e, global geometric stiffness K_G, and global load or pressure stiffness matrix K_P, the static criterion (divergence) for estimating load parameter λ_{cr} may be established through a linear eigenvalue analysis as follows

$$\left[\mathrm{K_e} - \lambda_{cr}(\mathrm{K_G} + \mathrm{K_P})\right]\Phi = 0 \tag{33}$$

λ_{cr} is the lowest eigenvalue and Φ is its associated eigenmode. As stated earlier, K_P is generally un-symmetric due to non-uniformity of loading and insufficient constraints in shell boundaries. In the sequel two types of eigenvalue analyses have been carried out, with pressure stiffness and without pressure stiffness. Comparison of the results of these two analyses to clarify the effects of considering or omitting K_P has been performed.

3. Numerical results and discussion

Based on the above derivations, lateral buckling pressure of different FGM conical shells with various geometries, boundary conditions, material properties are estimated. Specific attention has been paid on the effect of considering pressure stiffness matrix which stems in the follower action of pressure, on the buckling load**.** In all analyses, despite the un-symmetry of load stiffness matrix in some cases divergence-type failure mode has dominated in all cases.

3.1 Comparison results

In order to demonstrate the accuracy of present approach, Table 2 compares the static critical load for FGM conical shell and under lateral pressure with the results given by Sofiyev (2010). It is assumed that FGM shells are made of a mixture zirconium (ZrO_2) and titanium (Ti-6Al-4V). The properties of constituents, including the Young's modulus and Poisson's ratio are given in Table 1. Unless otherwise specified, the properties of the constituents are given at room temperature: T = 300 K.

According to the results in Table 2, the comparisons

Table 1 Material properties of FGMs from Reddy and Chin (2007)

Coefficients	ZrO_2		Ti-6Al-4V	
	E_c (MPa)	v_c	E_m (MPa)	v_m
F_0	2.4424×10^5	0.2882	1.2256×10^5	0.2884
F_{-1}	0	0	0	0
F_1	-1.371×10^{-3}	-1.133×10^{-4}	-4.586×10^{-3}	1.121×10^{-4}
F_2	1.214×10^{-6}	0	0	0
F_3	-3.681×10^{-9}	0	0	0
F	1.68063×10^5	0.298	1.056982×10^5	0.2981

Table 2 Variations of the values of critical load (MPa) for FGM conical shells with difference compositional profile, $\gamma = 45°$, $\frac{L}{R_1} = 2$

Materials	Uniform lateral pressure		Axial tension		Hydrostatic pressure		Hydrostatic pressure and axial tension	
N	Sofiev (2010)	Present study	Sofiev (2010)	Present study	Sofiev (2010)	Present study	Sofiev (2010)	Presentstudy
				$R_1/h = 100$				
ZrO_2	0.3169	0.2975	2.4412	2.3890	0.2993	0.2929	0.3047	0.3023
1	0.1761	0.1643	1.3594	1.3567	0.1663	0.1573	0.1693	0.1668
2	0.1665	0.1607	1.2778	1.2266	0.1573	0.1483	0.1601	0.1574
3	0.175	0.1712	1.3535	1.3245	0.1653	0.1582	0.1683	0.1650
Ti-6Al-4V	0.15903	0.1508	1.2249	1.1628	0.1502	0.1442	0.1529	0.1497
				$R_1/h = 200$				
ZrO_2	0.0554	0.0532	0.6132	0.5879	0.0534	0.0508	0.054	0.0527
1	0.0308	0.0305	0.3419	0.3315	0.0297	0.0287	0.03	0.0297
2	0.02914	0.0288	0.3203	0.3136	0.0281	0.0270	0.0284	0.0279
3	0.0306	0.0297	0.3407	0.3324	0.0295	0.0284	0.0298	0.0291
Ti-6Al-4V	0.0278	0.0266	0.3077	0.2993	0.0268	0.0257	0.0271	0.0264
				$R_1/h = 300$				
ZrO_2	0.0199	0.0191	0.2739	0.2650	0.0193	0.0185	0.0195	0.0189
1	0.011	0.0105	0.1527	0.1476	0.0107	0.0104	0.0108	0.0105
2	0.0104	0.0098	0.1431	0.1417	0.0101	0.0096	0.0102	0.0100
3	0.011	0.0105	0.1521	0.1491	0.0106	0.0104	0.0107	0.0105
Ti-6Al-4V	0.01	0.0095	0.1374	0.1350	0.0097	0.0096	0.0098	0.0095

show that the present results are in good agreement with those Sofiyev (2010).

3.2 Buckling results of FG cylindrical shells

In this problem the effects of considering pressure stiffness on buckling pressure in the clamped-clamped laminated cylindrical shell under uniform lateral pressure have been investigated. In this study the un-symmetry of pressure stiffness matrix due to shell boundaries and non-uniform loading effects disappears and apart from shell geometry static stability criterion dominates the problem. In addition, five different length to radius ratios which are 2, 4, 6, 8 and 10 as well as different thicknesses including 3.175, 6.35, 9.525 and 12.7 mm have been considered. Radius of the cylinder is 190.5 mm. The properties of constituents, including the Young's modulus and Poisson's ratio are given in Table 3.

Table 3 Mechanical properties of nickel and alumina in T = 300 K

Material	E (MPa)	v
Nickel	2.051×10^5	0.31
Alumina	3.20235×10^5	0.26

The relative difference of the buckling pressure for two states, without PS and with PS is estimated by Eq. (34).

$$\mu(\%) = \left| \frac{q_{cr(\text{without PS})} - q_{cr(\text{with PS})}}{q_{cr(\text{with PS})}} \right| * 100 \tag{34}$$

The buckling pressure against variation of power-law index of functionally graded material and geometry of the shell for follower forces, have been presented in Table 4.

Table 4 Buckling pressure (MPa) of cylindrical shell

				h = 3.175 mm			
L/R	N = 0	N = 0.5	N = 1	N = 5	N = 10	N = 30	N = 100
1	10.6440	11.0010	11.6900	12.2640	14.0600	15.2260	18.1360
2	5.1926	5.3615	5.6907	5.9712	6.8701	7.4423	8.8521
4	2.7393	2.8371	3.0217	3.1686	3.6039	3.9000	4.6612
6	1.8156	1.8788	1.9991	2.0966	2.3925	2.5899	3.0911
8	1.4926	1.5360	1.6242	1.7056	1.9869	2.1547	2.5495
10	1.1143	1.1512	1.2226	1.2827	1.4728	1.5952	1.8990
				h = 6.35 mm			
1	63.9810	66.3180	70.7060	74.1500	84.1430	91.0180	108.8200
2	28.7740	29.7420	31.6110	33.1690	38.0280	41.1740	49.0200
4	14.8450	15.3670	16.3580	17.1590	19.5630	21.1720	25.2690
6	10.2670	10.5910	11.2320	11.7920	13.6230	14.7590	17.5120
8	7.8247	8.1033	8.6301	9.0513	10.3030	11.1490	13.3160
10	7.0108	7.2737	7.7621	8.1370	9.1973	9.9467	11.9180
				h = 9.525 mm			
1	192.6600	199.9000	213.4000	223.8100	253.1800	273.7300	327.4900
2	82.4690	85.4610	91.0870	95.5330	108.5200	117.3900	140.2900
4	43.8230	45.1250	47.7650	50.1870	58.4130	63.1730	74.8330
6	27.7610	28.7370	30.5930	32.0950	36.6110	39.6170	47.2560
8	23.7730	24.6660	26.3240	27.5980	31.1940	33.7330	40.4110
10	21.0990	21.6850	22.9070	24.0830	28.2550	30.6350	36.0700
				h = 12.7 mm			
1	442.2200	459.7500	491.9100	515.7600	579.4000	625.9500	750.8500
2	165.3700	170.9700	181.8000	190.8500	218.9100	236.9200	281.7100
4	83.3470	86.0700	91.4030	95.9850	110.6000	119.7400	142.0800
6	59.9080	62.1100	66.2340	69.4620	78.7740	85.1980	101.8800
8	53.9940	56.0590	59.8720	62.7590	70.7530	76.4960	91.7420
10	38.2110	39.3950	41.7650	43.8840	50.8970	55.1240	65.2000

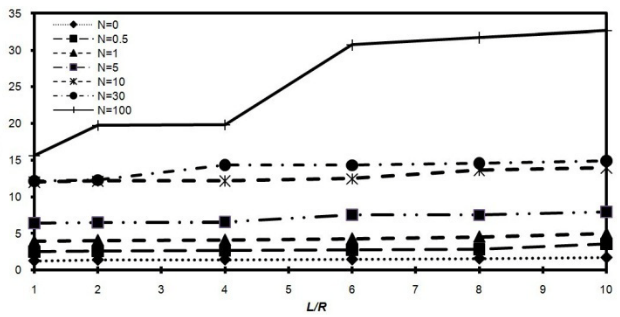

Fig. 7 The effect of follower force (μ) for h = 3.175 mm

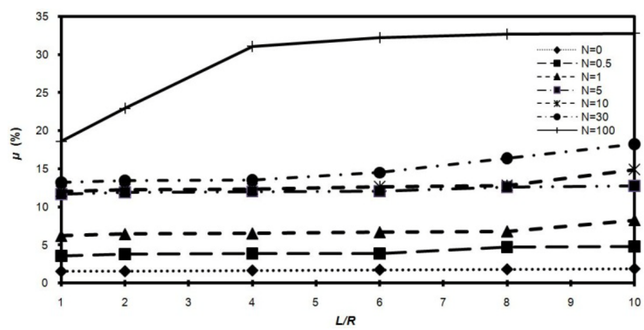

Fig. 8 The effect of follower force (μ) for h = 6.35 mm

It is found that, the critical buckling load increases with the increasing of N. As L/R ratio is increased, the values of critical load and corresponding circumferential wave number decrease for pure isotropic and FGM cylindrical shells with all compositional profiles. As L/R ratio increases, the estimated effects on the critical loads for the homogeneous and FG conical shells are nearly equal. When the values of critical loads of FGM cylindrical shells are compared with those of a homogeneous ceramic cylindrical shell, the least effect is encountered in N = 100 case, being 59% and the highest effect is encountered in N = 0.5, being l84%. The value of critical load with N = 100 (Alumina) is the greatest. The effects of N and length to radius ratios (L/R) on follower reduction coefficient (μ) for different thicknesses have been demonstrated in Figs. 7-10.

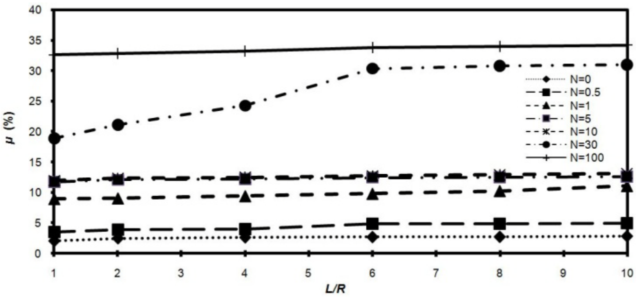

Fig. 9 The effect of follower force (μ) for h = 9.525 mm

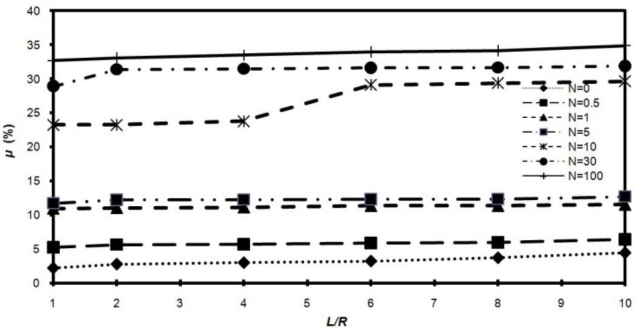

Fig. 10 The effect of follower force (μ) for h = 12.7 mm

By considering the presented results, it has been concluded when the loading is follower in the cylindrical shells, the calculated buckling load decreases rather than the state which the pressure is independent of deformations. The comparison of the results reveals that for both follower and non-follower states, the difference between calculated buckling loads depends on different factors such as shell geometry so that if the thickness or length to radius ratio increases, the differences escalate. According to Figs. 7-10 for all shell thickness variations, the minimum difference (μ) between follower and non-follower buckling pressure occurs at L/R = 1, while the maximum difference takes place at L/R = 10. Also, the obtained maximum difference happens when power-law index of functionally graded material, N, tends to 100. According to Figs. 7-10, it has been concluded that the maximum effect of follower force on the buckling load is nearly 35.73%. In other words, if the pressure stiffness matrix is neglected, shell is designed for a pressure nearly 35.73% smaller than the pressure which causes buckling.

3.3 Buckling results of FG conical shells

In this problem, the effects of follower action of loading on lateral buckling pressure of conical shell with different geometries and material properties are to be investigated. The boundary nodal line is fixed in the large base and free in the small base. Various apex angles and different shell thicknesses have been considered in the analyses. In this problem, we examined four pressure patterns (uniform lateral pressure, non-uniform longitudinal loading, non-

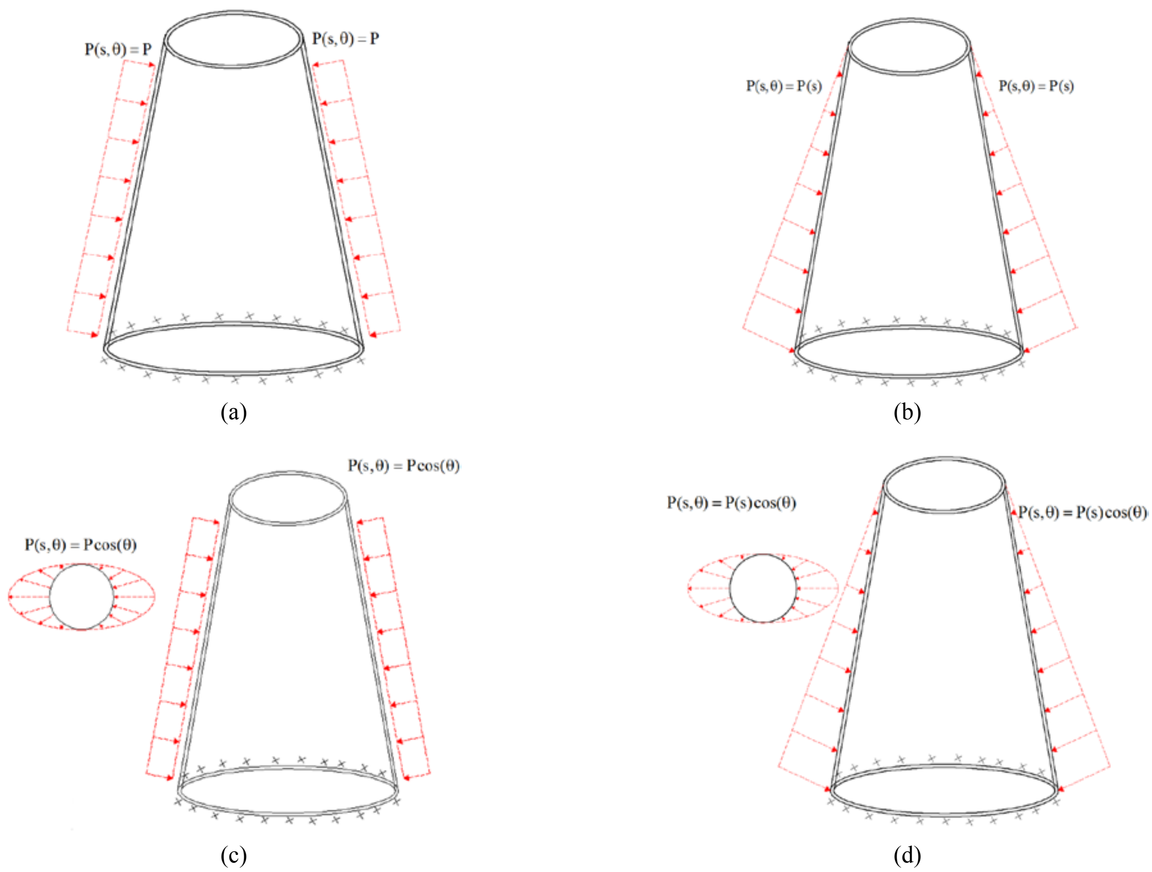

Fig. 11 Pressure patterns: (a) uniform lateral pressure; (b) non-uniform longitudinal loading; (c) non-uniform circumferential loading; (d) non-uniform longitudinal-circumferential loading)

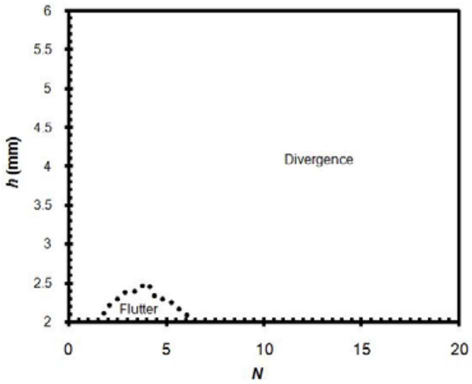

(a) Uniform loading $P(s, \theta) = P$

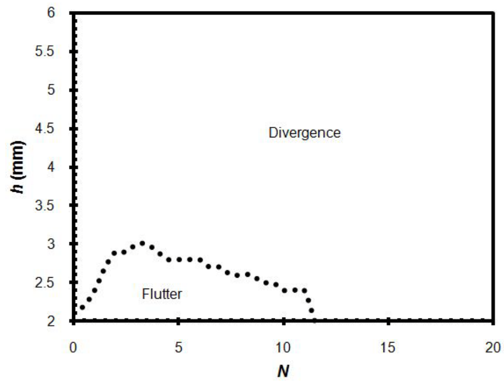

(b) Non-uniform loading $P(s, \theta) = P(s)$

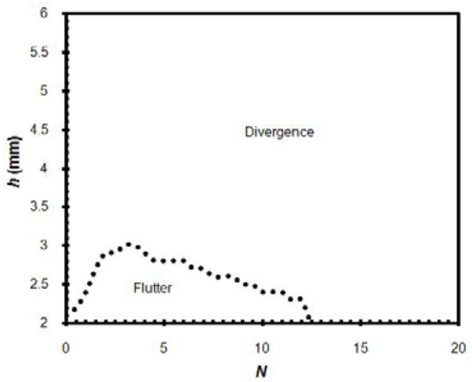

(c) Non-uniform loading $P(s, \theta) = P\cos(\theta)$

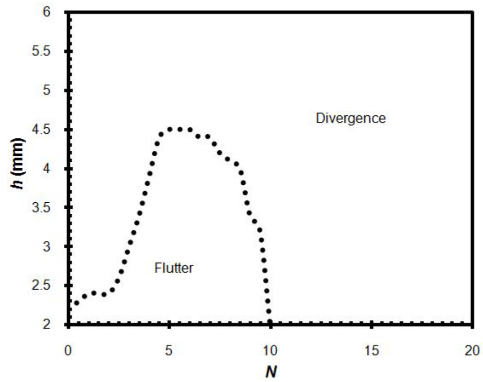

(d) Non-uniform loading $P(s, \theta) = P(s)\cos(\theta)$

Fig. 12 The transition curves from flutter to divergence for the FGM conical shell with $\gamma = 30°$

Table 5 Mechanical properties of nickel and alumina in $T = 300$ K

Material	E (MPa)	v
Stainless steel	2.07788×10^5	0.3176
Alumina	3.20235×10^5	0.26

uniform circumferential loading and non-uniform loading in both directions). The loading patterns have been depicted in Fig. 11.

Due to un-symmetry of pressure stiffness in the case of the loaded free boundary and non-uniform loading patterns and possibility of dominating either of divergence or flutter criteria, a primary analysis has been carried out to recognize the area of applicability of each method, especially static or divergence ones for three apex angles ($\gamma = 30°$, $45°$ and $60°$). Figs. 12-14 show the transition curves from flutter instability to divergence instability for various shells. In these diagrams, horizontal axis shows the power-law index of functionally graded material, N, while thickness of the shell is measured on the vertical axis. The region of the flutter instability was determined by using the dynamic stability analysis. The boundary between flutter and divergence instability passes always through a double critical point, where the first and second static (buckling) eigenmodes coincide (Zuo and Schreyer 1996). The properties of constituents, including the Young's modulus and Poisson's ratio are given in Table 5.

The geometric properties of the shell are $L/R_1 = 3$ and $R_1 = 100$ mm.

For the given shell subject to uniform and non-uniform distributed non-conservative forces, the boundary curves which separates divergence and flutter instability zones, have been found. The boundary curve has been created by a combination of power-law index of functionally graded material, N and shell thickness variation. For a specified N, thickness of the shell is varied until eigenvalue of the shell under follower lateral pressure based on static stability criterion becomes complex. Then this point, (N, h), is a point on the boundary curve. According to Figs. 12-14, the regions of flutter and divergence instability change by loading patterns. The largest and smallest regions of flutter instability have been induced by non-uniformity of loading in both directions, ($P(s, \theta) = P(s) \times \cos(\theta)$) and uniform pressure, respectively. The pattern of regions of instability changes by changing of semi-apex angle of truncated conical shell. Based on the results of primary analysis and the governing zones by the divergence criterion, several power-law indexes of FGM, N and three semi-apex angles of cone, γ, have been selected for the analyses. Thickness of the shell is 5 mm. The influences of aforementioned parameters on increasing or decreasing effect of follower action of lateral pressure on buckling capacity are shown in Figs. 15-18.

As the semi-vertex angle, γ, increases, the values of critical loads decrease for pure isotropic and FGM truncated conical shells with all compositional profiles. It is observed that for all loading patterns increasing in γ, decreases the

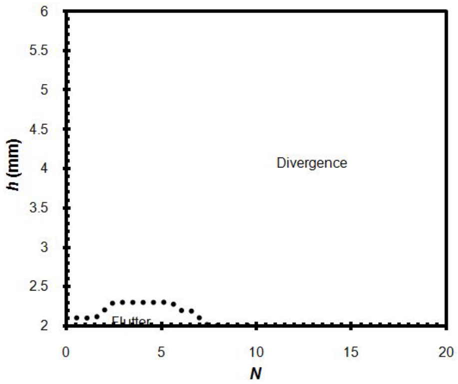

(a) Uniform loading $P(s, \theta) = P$

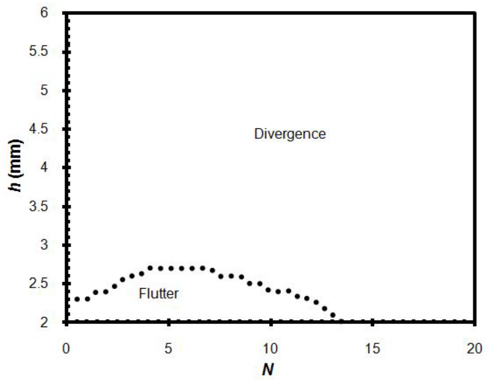

(b) Non-uniform loading $P(s, \theta) = P(s)$

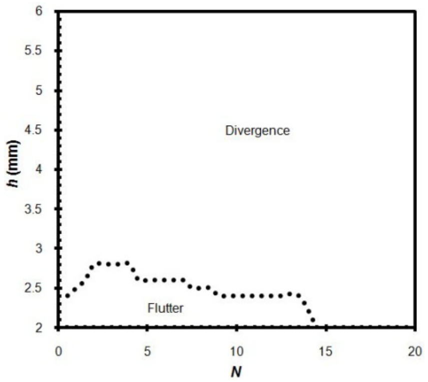

(c) Non-uniform loading $P(s, \theta) = P\cos(\theta)$

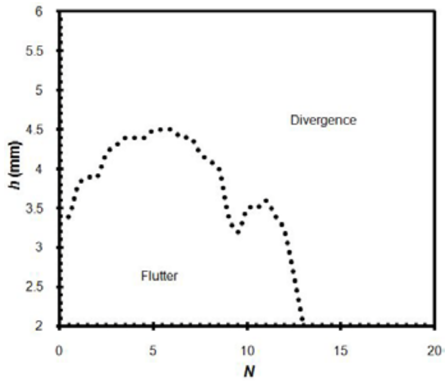

(d) Non-uniform loading $P(s, \theta) = P(s)\cos(\theta)$

Fig. 13 The transition curves from flutter to divergence for the conical $\gamma = 45°$

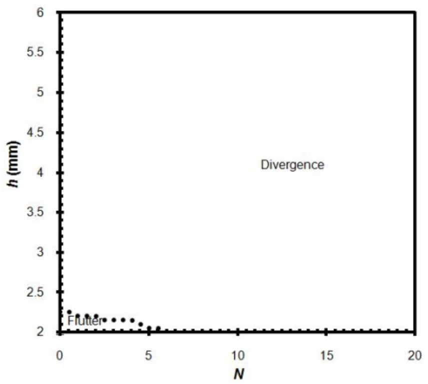

(a) Uniform loading $P(s, \theta) = P$

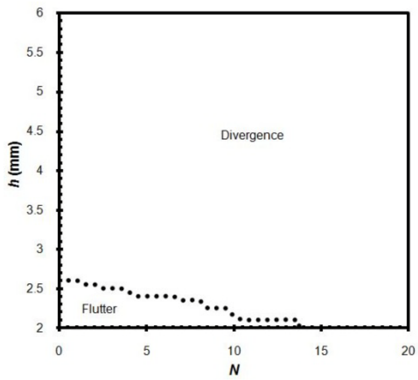

(b) Non-uniform loading $P(s, \theta) = P(s)$

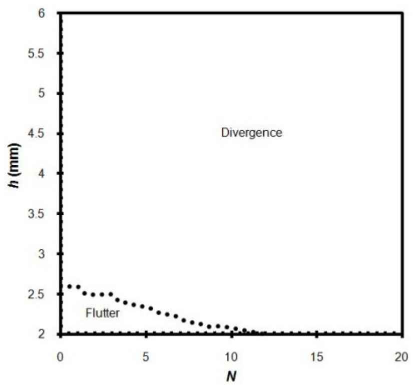

(c) Non-uniform loading $P(s, \theta) = P\cos(\theta)$

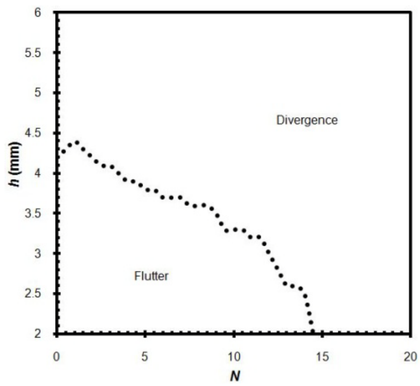

(d) Non-uniform loading $P(s, \theta) = P(s)\cos(\theta)$

Fig. 14 The transition curves from flutter to divergence for the conical $\gamma = 60°$

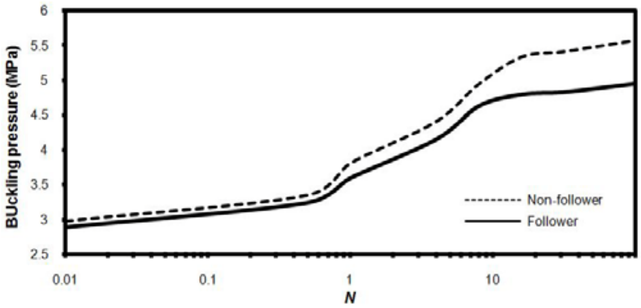

(a) $\gamma = 30°$

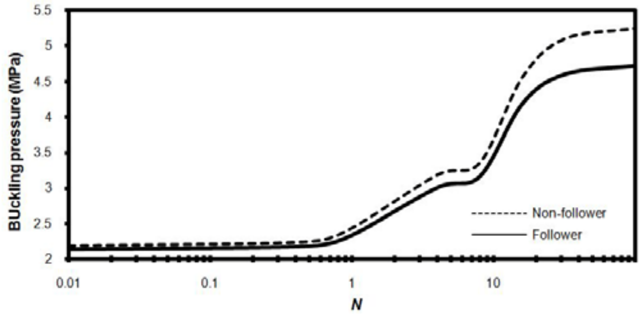

(b) $\gamma = 45°$

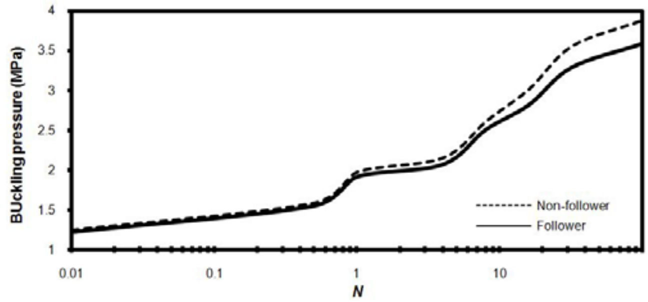

(c) $\gamma = 60°$

Fig. 15 Variations of uniform lateral buckling pressure for FGM conical shell

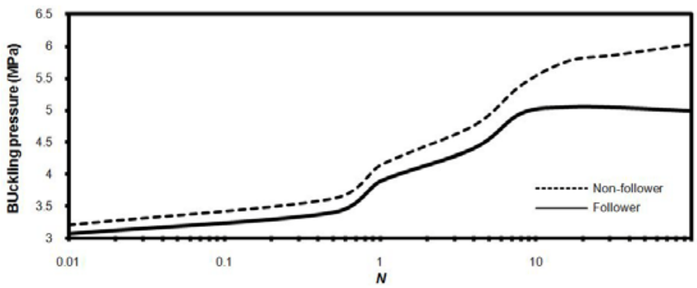

(a) $\gamma = 30°$

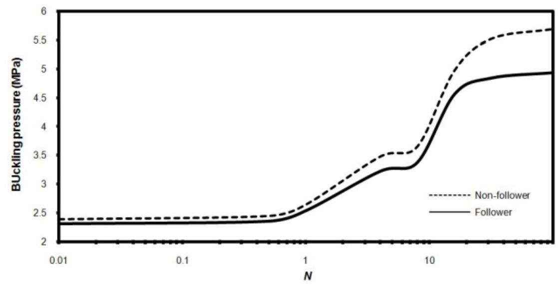

(b) $\gamma = 45°$

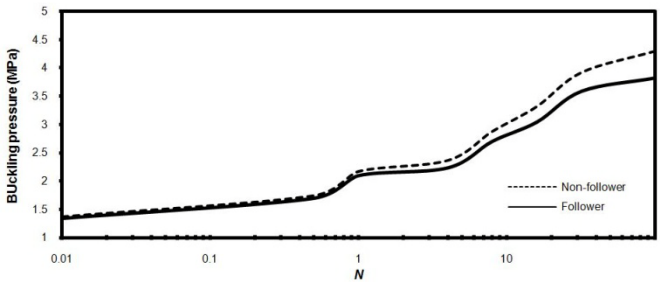

(c) $\gamma = 60°$

Fig. 16 Variations of non-uniform ($P(s, \theta) = P(s)$) lateral buckling pressure for FGM conical shell

influence of follower action. For all N, thickness and γ angle, non-uniform pressure causes more reducing effect on buckling pressure due to follower action than uniform pressure. It is seen that critical loads of pressure distribution, $P(s, \theta) = P(s)\cos(\theta)$ are higher than those of $P(s,\theta) = P\cos(\theta)$, $P(s, \theta) = P(s)$ and uniform pressures, whereas, the buckling pressures of $P(s, \theta) = P(s)$ are higher than the values of critical uniform pressures of the truncated conical shell. Furthermore, the uniform buckling pressures, follower and non-follower are lower than those of patterns $P(s, \theta) = P\cos(\theta)$ for the truncated conical FGM shell. The maximum differences between uniform buckling pressure and those of other patterns, ($P(s)$, $P(\theta)$ and $P(s, \theta)$) are 9% , 12% and 14%, respectively. Also, it can be concluded that thickness escalation in the case of $\gamma < 45$, has the most effect on buckling load reduction due to taking follower effect into account. As the semi-vertex angle, γ, increases, the differences between follower and non-follower lateral

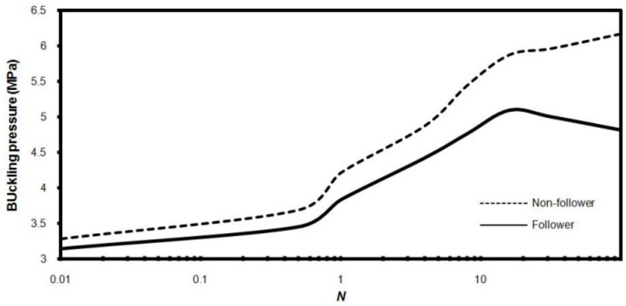

(a) $\gamma = 30°$

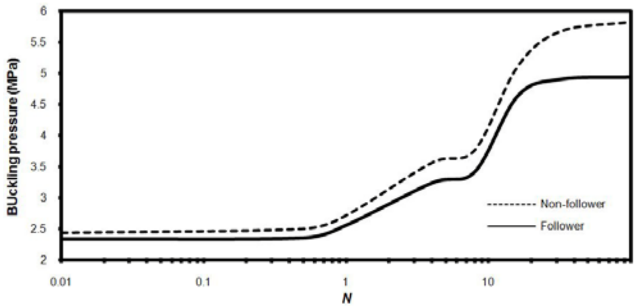

(b) $\gamma = 45°$

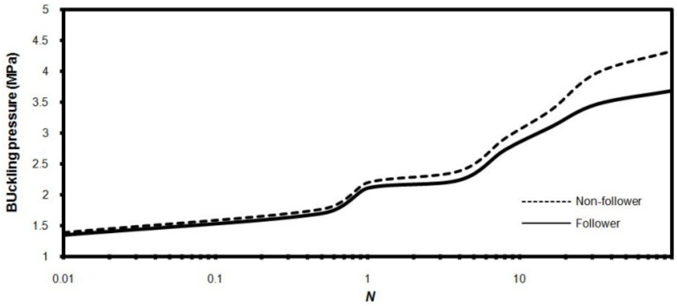

(c) $\gamma = 60°$

Fig. 17 Variations of non-uniform ($P(s, \theta) = P\cos(\theta)$) lateral buckling pressure for FGM conical shell

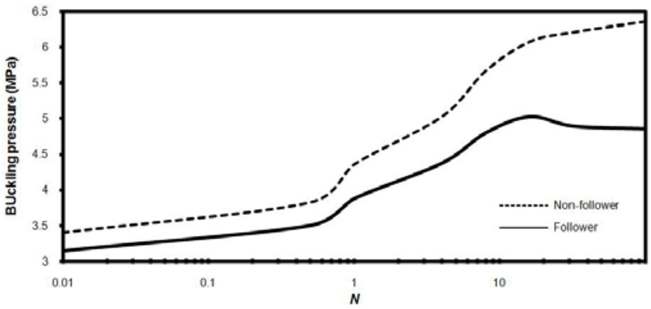

(a) $\gamma = 30°$

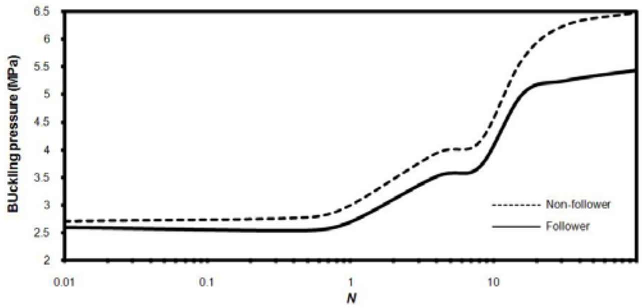

(b) $\gamma = 45°$

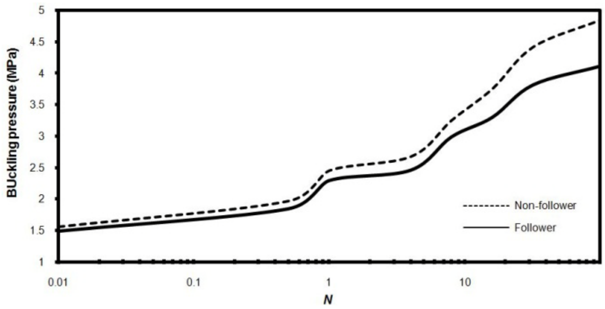

(c) $\gamma = 60°$

Fig. 18 Variations of non-uniform ($P(s, \theta) = P(s)\cos(\theta)$) lateral buckling pressure for FGM conical shell

buckling pressures for metal, ceramic and FGM conical shells with all compositional profiles decrease.

4. Conclusions

In this study, the eign buckling analysis of FGM truncated conical shells under lateral pressure follower have been investigated. The effects of various pressures patterns including follower and non-follower types and uniform and non-uniform distributions on the shell buckling have been estimated. The pressure stiffness matrix induced by the follower pressure was derived and categorized into three parts, a symmetric and two skew-symmetric matrices. The symmetric part reflects the shell domain integral and the other two skew-symmetric matrices involve the unconstrained boundaries and load non-uniformity effects. In the present study uniform and non-uniform lateral pressures, follower and non-follower types were taken into account. So, un-symmetry due to unconstrained boundaries and loading patterns can present in the analyses. Despite un-symmetry of pressure stiffness matrix in some cases, all analyses were based on divergence criterion and so only static stability analysis was carried out. A parametric study including various shell shapes, different boundary conditions, several shell geometries and various functionally graded materials with follower action of lateral pressure were carried out. The numerical results support the following conclusions:

- All of the assumptions in this paper result in a reasonable accuracy for different shells, loadings, materials in presence or absence of the pressure stiffness effect.
- The results for functionally graded material truncated conical shells show, when the pressure stiffness effect is included, this effect can result in reduction of the critical load as calculated without this effect. Therefore, it is considered that the assumption of loads which remain constant direction during deformations can lead to inaccurate results.
- Apart from any geometry, boundary conditions and material properties the effect of follower action of lateral pressure on buckling load diminishes with increasing in cone apex angle.
- The circumferential wave number can be a sign for considerable or negligible effect of follower action of lateral pressure. The maximum influence is along with small circumferential wave number which definitely the shell geometry, boundary conditions and material properties play essential role in it.
- The regions of flutter and divergence dominant stability criteria have been formed combination of power-law index of functionally graded material, N and shell thickness variations. These regions change with the assumed loading patterns.

References

ABAQUS/standard user's manual (1998), Vols. I-III, Version 5.8; Hibbitt, Karlsson & Sorensen, Inc., Pawtucket, RI, USA.

Argyris, J.H. and Symeonidis, Sp. (1981), "Nonlinear finite element analysis of elastic system under nonconservative loading – natural formulation, part1, quasistatic problems", *Comput. Methods Appl. Mech. Eng.*, **26**(1), 75-123.

Altman, W. and Oliveira, M.G.D. (1988), "Vibration and Stability cantilevered cylindrical shell panels under follower forces", *J. Sound Vib.*, **122**(2), 291-298.

Altman, W. and Oliveira, M.G.D. (1990), "Vibration and Stability shell panels with slight internal damping under follower forces", *J. Sound Vib.*, **136**(1), 45-50.

Altman, W. and Oliveira, M.G.D. (1987), "Stability of cylindrical shell panels subjected to follower forces based on a mixed finite element formulation", *Comput. Struct.*, **27**(3), 367-372.

Bich, D.H., Ninh, D.G. and Tran, I.T. (2016), "Non-linear buckling analysis of FGM toroidal shell segments filled inside by an elastic medium under external pressure loads including temperature effects", *Compos. Part B*, **87**, 75-91.

Bolotin, V.V. (1963), *Nonconservative Problems of the Theory of Elastic Stability*, Pergamon Press, New York, NY, USA, pp. 53-55.

Cagdas, I.U. and Adali, S. (2011), "Buckling of cross-ply cylinders under hydrostatic pressure considering pressure stiffness", *Ocean Eng.*, **38**(4), 559-569.

Carnoy, E.G., Guennoun, N. and Sander, G. (1984), "Static buckling analysis of shell submitted to follower force by finite elment method", *Comput. Struct.*, **19**(1-2), 41-49.

Chi, S.H. and Chung, Y.L. (2006), "Mechanical behavior of functionally graded material", *Int. J. Solids Struct.*, **43**(13), 3657-3674.

Chaht, F.L., Kaci, A., Houari, M.S.A., Tounsi, A., Bég, O.A. and Mahmoud, S.R. (2015), "Ending and buckling analyses of functionally graded material (FGM) size-dependent nanoscale beams including the thickness stretching effect", *Steel Compos. Struct., Int. J.*, **18**(2), 425-442.

Cohen, G.A. (1966), "Conservative of a normal pressure field acting on a shell", *AIAA*, **4**(10), 1886-1886.

Datta, P.K. and Biswas, S. (2011), "Aeroelastic behaviour of aerospace structural Elements with Follower Force: A review", *J. Aeronaut. Space Sci.*, **12**(2), 134-148.

Dung, D.V. and Hoa, L.K. (2015), "Nonlinear torsional buckling and postbuckling of eccentrically stiffened FGM cylindrical shells in thermal environment", *Compos.: Part B*, **69**, 378-388.

Duc, N.D., Thang, P.T., Dao, N.T. and Tac, H.V. (2015), "Nonlinear buckling of higher deformable S-FGM thick circular cylindrical shells with metal-ceramic-metal layers surrounded on elastic foundations in thermal environment", *Compos. Struct.res*, **121**, 134-141.

Fantuzzi, N., Brischetto, S., Tornabene, F. and Viola, E. (2016), "2D and 3D shell models for the free vibration investigation of functionally graded cylindrical and spherical panels", *Compos. Struct.,* **154**, 573-590.

Ganapathi, M. (2007), "Dynamic stability characteristics of functionally graded materials shallow spherical shells", *Compos. Struct.*, **79**(3), 338-343.

Goyal, V.K. and Kapania, R.K. (2008), "Dynamic stability of laminated beams subjected to non-conservative loading", *Thin-Wall. Struct.*, **46**(12), 1359-1369.

Hibbitt, H.D. (1979), "Some follower forces and load stiffness", *Int. J. Numer. Methods Eng.*, **14**(6), 207-231.

Iwata, K., Tsukimor, K. and Kubo, F. (1991), "A symmetric load-stiffness matrix for buckling analysis of shell structures under pressure loads", *Int. J. Pres. Ves. & Piping*, **45**(1), 101-120.

Khayat, M., Poorveis, D., Moradi, S. and Hemmati, M. (2016), "Buckling of thick deep laminated composite shell of revolution under follower forces", *Struct. Eng. Mech., Int. J.*, **58**(1), 59-91.

Khayat, M., Poorveis, D. and Moradi, S. (2016), "Buckling analysis of laminated composite cylindrical shell subjected to lateral displacement-dependent pressure using semi-analytical finite strip method", *Steel Compos. Struct., Int. J.*, **22**(2), 301-321.

Lanhe, W. (2004), "Thermal buckling of a simply supported moderately thick rectangular FGM plate", *Compos. Struct.*, **64**(2), 211-218.

Loganathan, K., Chan, S.C., Gallagher, R.H. and Abel, J.F. (1979), "Finite element representation and pressure stiffness in shell stability analysis", *Int. J. Numer. Methods Eng.*, **14**(9), 1413-1429.

Na, K.S. and Kim, J.H. (2004), "Three-dimensional thermal buckling analysis of functionally graded materials", *Compos.: Part B*, **35**(5), 429-437.

Poorveis, D. and Kabir, M.Z. (2006), "Buckling of discretely stringer-stiffened composite cylindrical shells under combined axial compression and external pressure", *Scientia Iranica*,

13(2), 113-123.

Rasheedat, M.M. and Akinlabi, E.T. (2012), "Functionally Graded Material: An overview", *Proceedings of the World Congress on Engineering,* London, UK, July.

Reddy, J.N. and Chin, C.D. (2007), "Thermo mechanical analysis of functionally graded cylinders and plates", *J. Therm. Stresses*, **21**(6), 593-626.

Sanders, J.L. (1963), "Nonlinear theories for thin shells", *Quarterly J. Appl. Math*, **21**(1), 21-36.

Santos, H., Soares, C.M.M., Soares, C.A.M. and Reddy, J.N. (2008), "A semi-analytical finite element model for the analysis of cylindrical shells made of functionally graded materials under thermal shock", *Compos. Struct.*, **86**(1-3), 10-21.

Schweizerhof, K. and Ramm, E. (1984), "Displacement dependent pressure loads in nonlinear finite element analysis", *Comput. Struct.*, **18**(6), 1099-1114.

Shen, H.S. (2002), "Postbuckling analysis of axially-loaded functionally graded cylindrical shells in thermal environments", *Compos. Sci. Technol.*, **62**(7-8), 977-998.

Sofiyev, A.H. (2010), "The buckling of FGM truncated conical shells subjected to combined axial tension and hydrostatic pressure", *Compos. Struct.*, **92**(2), 488-498.

Torki, M.E., Kazemi, M.T., Haddadpour, H. and Mahmoudkhani, S. (2014), "Dynamic stability of cantilevered functionally graded cylindrical shells under axial follower forces", *Thin-Wall. Struct.*, **79**, 138-146.

Tornabene, F. (2011) "2-D GDQ solution for free vibrations of anisotropic doubly-curved shells and panels of revolution", *Compos. Struct.*, **93**(7), 1854-1876.

Tornabene, F., Fantuzzi, N. and Bacciocchi, M. (2014), "Free vibrations of free-form doubly curved shells made of functionally graded materials using higher order equivalent single later theories", *Compos.: Part B*, **67**, 490-509.

Zhang, Y., Huang, H. and Han, Q. (2015), "Buckling of elastoplastic functionally graded cylindrical shells under combined compression and pressure", *Compos.-Part B*, **69**, 120-126.

Zuo, Q.H. and Schreyer, H.L. (1996), "Flutter and divergence instability of nonconservative beams and plates", *Int. J. Solids Struct.,* **33**(9), 1355-1367.

Viola, E., Rossetti, L., Fantuzzi, N. and Tornabene, F. (2016), "Generalized stress-strain recovery formulation applied to functionally graded spherical shells and panels under static loading", *Compos. Struct.*, **156**, 145-164.
DOI: 10.1016/j.compstruct.2015.12.060

Wang, Q. (2003), "On complex flutter and buckling analysis of a beam structure subjected to static follower force", *Struct. Eng. Mech*., *Int. J.,* **16**(5), 533-556.

CC